PCCP

PAPER

Cite this: *Phys. Chem. Chem. Phys.*, 2017, **19**, 24915

Quantum dots in photocatalytic applications: efficiently enhancing visible light photocatalytic activity by integrating CdO quantum dots as sensitizers†

A. H. Reshak

The amalgamation of a wide optical band gap photocatalyst with visible-light-active CdO quantum dots (QDs) as sensitizers is one of the most efficient ways to improve photocatalytic performance under visible light irradiation. The photocatalytic performance of cadmium benzoate ($((Cd(C_7H_5O_2)_2)_3(CH_3CN)_1)$) is comprehensively investigated. The estimated optical band gap of cadmium benzoate is 2.64 eV and the EPc and EPv are about −0.09 V (*vs.* NHE) and +2.55 V (*vs.* NHE), respectively, which implies that cadmium benzoate possesses a high negative reduction potential of excited electrons due to its higher conduction band position, and hence, the locations of the conduction band minimum and the valence band maximum meet the redox capacity. Thus, this composite photocatalyst exhibits superior activity in visible-light-driven photocatalytic H_2 evolution. We found that introducing the QDs enhance the photocatalytic performance towards the visible light region. The electronic band structure shows high *k*-dispersion bands around the Fermi level, which implies low effective masses, and hence, the high mobility carriers favor the enhancement of the charge transfer process. The mobility of the photogenerated carriers significantly influences the photocatalytic efficiency and the higher photogenerated carriers' mobility enhances the photocatalytic performance. Moreover, the result shows a great effective mass difference between electrons (e^-) and holes (h^+), which can facilitate the e^- and h^+ migration and separation, and finally improve the photocatalytic performance. The large mobility difference is useful for the separation of e^- and h^+, the reduction of the e^- and h^+ recombination rate, and the improvement of the photocatalytic activity. Thus, cadmium benzoate exhibits rapid generation of e^-–h^+ pairs with photoexcitation and a high negative reduction potential of excited electrons due to its higher CB position. Based on these results one can conclude that cadmium benzoate satisfied all requirements to be an efficient photocatalyst. This will greatly improve the search efficiency and greatly help experimentalists in saving resources in the exploration of new photocatalysts with good photocatalytic performance.

Received 5th August 2017,
Accepted 25th August 2017

DOI: 10.1039/c7cp05312f

rsc.li/pccp

1. Introduction

Since semiconductor-based water splitting was discovered, the application of wide band gap semiconductors in photocatalysis continues to face major obstacles, namely (i) poor response to visible light, owing to their wide energy band gaps, and (ii) low utilization of light absorbed, due to the high recombination of photogenerated carriers.[1] Regardless of efforts made towards improving the photocatalytic properties of wide band gap semiconductors, the existing modification strategies, including morphology optimization, foreign element doping, dye sensitization, and metal deposition, among others, still fall short of achieving these improved properties.[2,3] One of the promising modification strategies is the amalgamation of wide energy band gap semiconductors with visible-light-active quantum dots (QDs). This promise has been claimed due to its advantages in strengthening charge transport and reducing recombination of photogenerated carriers, while simultaneously extending the light absorption range.[4,5] It is interesting to mention that the investigation of incorporating Au and/or CdS NPs as co-catalysts or sensitizers has shown the technique to be highly effective in improving the photocatalytic activity of wide band gap semiconductor photocatalysts like TiO_2, especially in the visible light region.[6–15] It is important to highlight that, for the resulting composite photocatalysts, the electron transfer trajectory under visible irradiation is often different from that under UV irradiation. For instance, in the photocatalytic process in Au/TiO_2 under UV irradiation, the

New Technologies – Research Centre, University of West Bohemia, Univerzitni 8, 306 14 Pilsen, Czech Republic. E-mail: maalidph@yahoo.co.uk; Fax: +420-386 361255; Tel: +420-777 729583

† Electronic supplementary information (ESI) available. See DOI: 10.1039/c7cp05312f

photogenerated electrons transfer from TiO_2 to Au and the reduction reaction occurs around the surface of the Au NPs deposited on TiO_2.[16–18] In contrast, the electron transfer trajectory would be reversed under visible light irradiation, *i.e.*, from Au to TiO_2.[19]

Nanoscale semiconductors have received great attention due to their unique structural, optical and electronic properties. These unique properties are due to their large surface area-to-volume ratios and quantum confinement effects. The increase of the surface area-to-volume ratio changes the mechanical, optical, chemical, thermal and catalytic properties of the materials significantly. One of the interesting nanoscale semiconductors is quantum dots (QDs), which are zero-dimensional (0-D) semiconductor nanomaterials. QDs are confined to a size of 2–8 nm in 3-D, and are defined as particles with physical dimensions smaller than the exciton Bohr radius.[20] In recent years, the synthesis of various sizes and shapes of nanoparticle semiconductors doped with different dopants to be used as efficient nanophotocatalysts has become an attractive research field.[21] Photocatalysis is a green technique that has been widely applied in the fields of environmental remediation and solar water splitting.[22–24] Recently, there have been numerous studies on photocatalytic H_2 production and a series of semiconductor photocatalysts that include metal oxides, nitrides, titanates, and niobates,[25–30] where high photocatalytic activities for H_2 production have been reported. In recent years, much attention has been given to the research field of nano-crystalline oxide materials due to their potential importance and the wide range of technological applications.[31–36] It has been reported that CdO is a degenerate n-type semiconductor used in optoelectronic applications, for instance, in photovoltaic cells,[37] solar cells,[38] phototransistors,[39] infra-red reflectors,[40] transparent electrodes[41] and gas sensors.[32,42,43] These applications are based on its unusual optical and electrical properties.[44] CdO crystallizes in a non-centro-symmetric structure; thus, it is very interesting to highlight that the non-centro-symmetric structure induces a spontaneous polarization due to the displacement of the centers of the positive and negative charges in a unit cell.[45] Because their positive and negative charges have different centers of symmetry, non-centro-symmetric materials belong to ferroelectric materials that have a macroscopic polarization which induces the accumulation of charges at the surfaces.[16] Thus, a spontaneous polarization can be screened by free electrons (e^-) in the CB and free holes (h^+) in the VB, and/or by ions adsorbed on the surface from the solution forming a Stern layer.[46] A positive charge in positive fields is screened by external and internal mechanisms.[47] The internal mechanism forms a negatively charged region below the surface, and the external mechanism consists of the adsorption of foreign negatively charged ions at the surface. On the other hand, the opposite reactions take place in negative fields, and the adsorbed foreign ions are positively charged. This charge reallocation generates an electric field around the charged region.[48] A polarization field is compensated at equilibrium by the screening mechanisms. Thus, the photogenerated electrons can easily migrate to the surface and give rise to oxidation and reduction products at different locations.[17] This in turn enhances the photocatalytic activity. We should emphasize that the unique photochemistry of non-centrosymmetric materials may be utilized to launch some new photoreaction pathways. Moreover, the Cd–O units possess strong electron cloud overlap and prefer to attract h^+ and repel e^-, thus facilitating the separation of the photogenerated e^-–h^+ pairs. This in turn enhances the photocatalytic activity. It is interesting to highlight that the polarizability lowers the potential energy of charged particles and transition states regardless of whether these particles are negatively or positively charged.[18]

The problems of energy shortages and environmental crises motivated several researchers to find alternative energy resources. Photocatalysts are one of the promising alternatives for clean and environment-friendly energy production.[49–51] Utilizing solar light irradiation, photocatalysts can be used to decompose organic contaminants for environmental purification and split water into hydrogen and oxygen. Great efforts have been made towards growing high quality crystals to enhance the photocatalytic performance, and towards discovering novel crystals with excellent photocatalytic properties, which can be generally classified as oxides,[52] sulfides,[53] oxysalts,[54] polymers[55] and quantum dots.[56–58] Quantum dots show high photostability and a tunable absorption spectrum; thus, semiconductor quantum dots have the potential for use as photosensitizers in photocatalysis. A quantum dot can be used to transfer a hole upon photoexcitation to a water oxidation catalyst, so that the catalyst can drive the water splitting reaction. Similarly, quantum dots could be used to transfer electrons to a proton reduction catalyst to make molecular hydrogen as a solar fuel. The ultimate goal is to have multiple charges transferred from one quantum dot to one electron or hole acceptor. However, it is still desirable to find materials with promising photocatalytic properties; the search for a better candidate has not ceased. Therefore, we provide a detailed depiction of the electronic structure and transport, photocatalytic and optical properties of cadmium benzoate ($(Cd(C_7H_5O_2)_2)_3(CH_3CN)_1$) using the full-potential method, which is timely and would bring us important insights into understanding the origin of the band structure, density of states, and photocatalytic and photophysical properties. Hence, it is very important to use a full-potential method based on density functional theory (DFT). The full-potential method[59] within the general gradient approximation (PBE-GGA)[60] and the modified Becke–Johnson potential (mBJ)[61] are used to ascertain the influence of the XC on the resulting band gap, and hence on the ground-state properties of cadmium benzoate ($(Cd(C_7H_5O_2)_2)_3(CH_3CN)_1$). The unique properties of QDs make them efficient semiconductor nanophotocatalysts, especially for environmental applications.

In this work, *ab initio* calculations from first- to second-principles methods are performed to investigate the suitability of cadmium benzoate ($(Cd(C_7H_5O_2)_2)_3(CH_3CN)_1$) for use as active photocatalysts in the visible light region. It is well known that the DFT approaches have the ability to accurately predict the ground state properties of the materials, and the developed analysis tools are vital to investigating their intrinsic mechanism. This microscopic understanding has further guided molecular engineering design for new materials with novel structures and properties. It is anticipated that first-principles material

approaches will greatly improve the search efficiency and greatly help experimentalists in saving resources in the exploration of new crystals with good performance.[62–68] For instance, several researchers have used first-principles calculations to explore new photocatalysts and found good agreement with the experimental results.[64–70] We would like to mention that, in our previous works,[69–72] we have calculated the energy band gaps and the photocatalytic properties using the full potential method for several systems whose energy band gaps and photocatalytic properties are known experimentally and a very good agreement with the experimental data was obtained. Thus, we believe that our calculations reported in this paper would produce very accurate and reliable results which greatly will help experimentalists in saving resources in the exploration of new photocatalysts with good photocatalytic performance. The aim of this work is to focus on the photocatalytic activity of QDs as new, green and efficient nanophotocatalysts.

2. Methodology

Cadmium benzoate ($(Cd(C_7H_5O_2)_2)_3(CH_3CN)_1$) crystallizes in monoclinic symmetry with '$P121/c1$' (no. 14). The experimental lattice parameters are a = 17.0374 (12) Å, b = 9.1839 (6) Å, c = 26.2103 (18) Å and Z = 4.[56] As the first step a geometrical relaxation was performed for the experimental X-ray diffraction of cadmium benzoate ($(Cd(C_7H_5O_2)_2)_3(CH_3CN)_1$)[56] using the Perdew–Burke–Ernzerhof generalized gradient approximation (PBE-GGA).[60] The relaxed geometry of ($(Cd(C_7H_5O_2)_2)_3(CH_3CN)_1$) in comparison with the experimental data[56] is provided in the ESI.† A good agreement was found between the relaxed geometry and the experimental data. The relaxed geometry is shown in Fig. 1. Using the obtained relaxed geometry, the electronic band structure, density of states, electron charge density distribution, and transport and photocatalytic properties are calculated using the all-electron full-potential linear augmented plane wave (FPLAPW + lo) method as embodied in the Wien2k code,[59] utilizing the modified Becke–Johnson potential (mBJ) to treat the exchange correlation.[61] The mBJ is a local approximation of an atomic ''exact-exchange'' potential and a screening term which allows the calculation of band gaps with accuracy similar to the very expensive GW calculations.[61] We would like to mention that in our previous works we calculated the energy band gap using the FPLAPW method within mBJ on several systems whose energy band gaps are known experimentally; in those previous calculations we found very good agreement with the experimental data. Thus, we believe that our calculations reported in this paper would produce very accurate and reliable results. The muffin-tin radii (R_{MT}) of Cd, N, O, C and H atoms were chosen in such a way that the spheres did not overlap. The R_{MT} value is taken to be 2.07 a.u. (Cd), 1.04 a.u. (N), 1.17 a.u. (O), 0.99 a.u. (C) and 0.59 a.u. (H). To achieve the total energy convergence, the basis functions in the interstitial region were expanded up to $R_{MT} \times K_{max}$ = 7.0. The maximum value of l was taken as l_{max} = 10, while the charge density is Fourier expanded up to G_{max} = 12 $(a.u)^{-1}$. Self-consistency is obtained using 1000 $\vec{k}$ points in the irreducible Brillouin zone (IBZ). The self-consistent calculations are converged when the total energy of the system is stable within 0.00001 Ry. The calculations of the electronic band structure, density of states and electronic charge density distribution are performed with 3500 $\vec{k}$ points in the IBZ. In this study we provide the details of the investigation concerning the suitability of cadmium benzoate for use as an efficient photocatalyst under visible irradiation utilizing the first-principles material approaches, which greatly improve the search efficiency and greatly help experimentalists in saving resources in the exploration of new photocatalysts with good photocatalytic performance.

3. Results and discussion

3.1. Structure–property relationship

Since the photocatalytic activities are directly related to the material's electronic structure,[73] the electronic band structure of cadmium benzoate ($(Cd(C_7H_5O_2)_2)_3(CH_3CN)_1$) along the high symmetry directions of the first BZ is calculated to explore the bands' dispersion and the nature of the fundamental energy band gap, as shown in Fig. 2a. We set the zero-point of energy (Fermi level, E_F) at the valence band maximum (VBM). It has been found that the conduction band minimum (CBM) is situated between the Z and Γ points of the BZ, whereas the VBM is located between the Z and Y points, resulting in an indirect energy band gap of about 3.4 eV. Therefore, the electrons (e^-) cannot recombine directly with holes (h^+); this needs instead the assistance of phonons in order to maintain momentum conservation.[74–76] This implies that the investigated material may have a long lifetime of photoexcited e^- and h^+, which can increase the probabilities for photogenerated e^- and h^+ to participate in photocatalytic reactions. Moreover, the QDs possess a higher surface area-to-volume ratio than their bulk counterparts, and thus allow for greater photon absorption on the photocatalyst surface, and the recombination of the e^- and h^+ pairs drastically decreases as the size of the QDs decreases. Therefore, QD semiconductors are expected to show higher photocatalytic activity than their bulk.[77] To explore the types of orbitals which form the CBM and the VBM, the total and partial densities of states are investigated as shown in Fig. 2b–f. These figures reveal that the VBM is mainly formed by O-2p states, whereas the CBM is formed by the Cd-4d and Cd-5s states. Therefore, introducing the QDs causes a significant band gap reduction which enhances the photocatalytic performance towards the visible light region. We would like to highlight that the CdO–cadmium benzoate ratio showed excellent efficiency[56] and the energy levels of CdO and CdB are sufficient to initiate the oxidiation or reduction reaction, and the formation of a heterojunction favors the enhancement of charge separation.[78–84] The relationship between the electrode potential for the CBM, VBM (EPc, EPv) and E_g can be expressed by the following equations:[85]

$$EPc\ (V\ vs.\ NHE) = 1.23 - E_g\ (eV)/2 \quad (1)$$

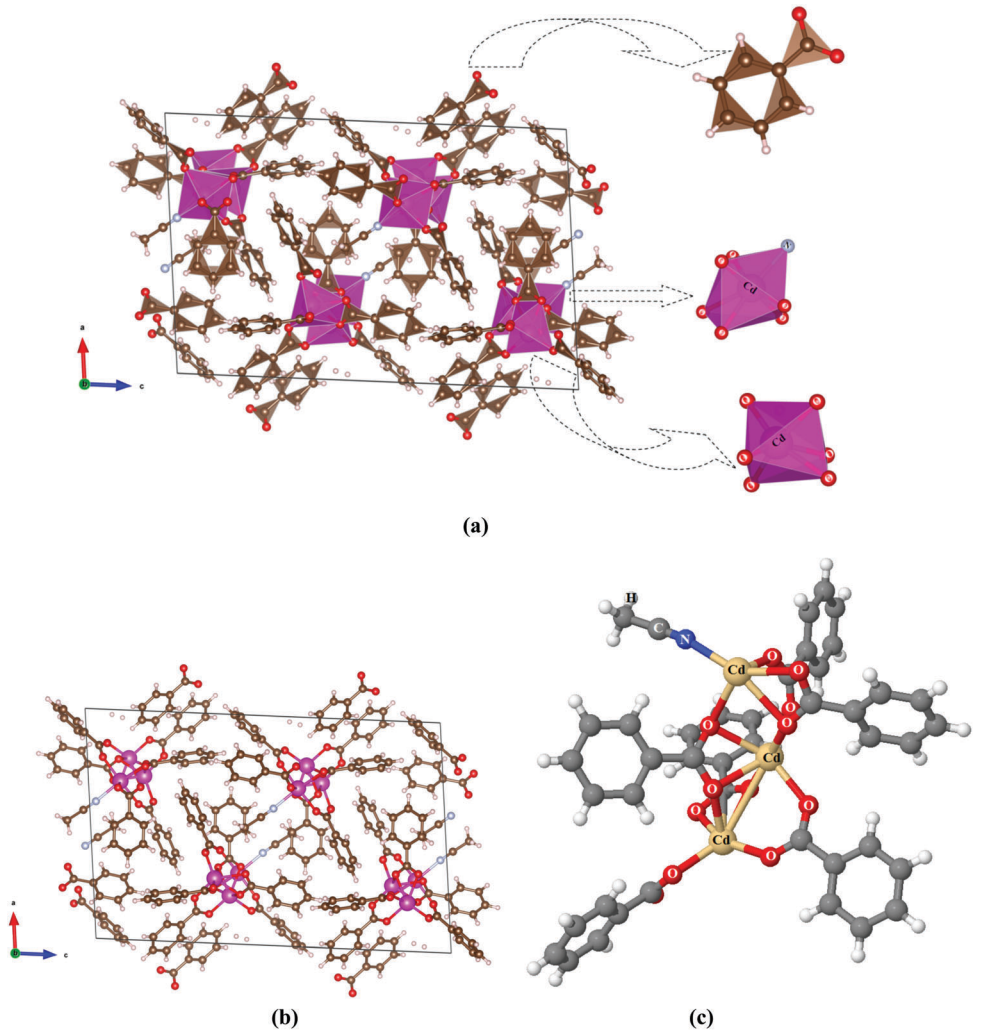

Fig. 1 (a and b) Crystal structures of cadmium benzoate ($(Cd(C_7H_5O_2)_2)_3(CH_3CN)_1$) with monoclinic symmetry with '*P*121/*c*1' (no. 14). The experimental lattice parameters are a = 17.0374 (12) Å, b = 9.1839 (6) Å, c = 26.2103 (18) Å and Z = 4. The crystal structure of cadmium benzoate ($(Cd(C_7H_5O_2)_2)_3(CH_3CN)_1$) forms through a combination of CdO quantum dots. These figures show only one unit cell which contains four formula units per unit cell, and (c) one formula unit.

$$\text{EPv (V } vs.\text{ NHE)} = 1.23 + E_g\text{ (eV)}/2 \quad (2)$$

The estimated optical band gap of cadmium benzoate ($(Cd(C_7H_5O_2)_2)_3(CH_3CN)_1$) is 2.64 eV; thus the EPc and EPv are about −0.09 V (*vs.* NHE) and +2.55 V (*vs.* NHE), respectively.

To realise the solar degradation of pollutants, the reduction capacity of e^- must be able to produce superoxide acid ($-HO_2$) and superoxide anion radicals ($-O^{2-}$), while the oxidation of the photogenerated holes (h^+) must be able to oxidize OH^- to produce reactive hydroxyl radicals (–OH).[86] The CBM for the photocatalyst material should increase to the vacuum level (EPc will be lower than H_2 + H/–HO_2 (*vs.* NHE) = −0.13 V). Simultaneously, the VBM should increase to a narrow energy band gap and maintain the oxidation capacity for h^+ (EPv lower than O_2/H_2O (*vs.* NHE = +1.23 V)). It is well known that –OH and $-O^{2-}$ are free radicals with high oxidation capacity; thus, –OH and $-O^{2-}$ can oxidize various organic and inorganic carbon compounds to produce dioxide, water and other non-toxic small organic molecules. Hence, the energy band gap of the photocatalyst determines the range of the solar spectrum absorbed. The narrower the energy band gap, the wider the spectral range response to solar radiation and the more efficiently it can make use of visible light. The locations of the CBM and VBM should meet the redox capacity.

Furthermore, in QDs, the transport length of e^-–h^+ from the crystal interface to the surface is short, which helps in accelerating the migration rate of e^-–h^+ to the QDs' surface in order to participate in the reaction process.[87] The short transport length and the increased accessible surface of photocatalysts as nanoparticles lead to increased photocatalytic activity of the QDs. The combination of QDs and wide band gap semiconductors facilitates the transport of charges photogenerated under visible light irradiation; the resulting composite photocatalyst exhibits superior activity in visible-light-driven photocatalytic H_2 evolution. Introducing QDs into wide energy band gap materials enhances the energy band gap; the width of the optical band gap is a very important factor for the photocatalyst, in other words, the range of

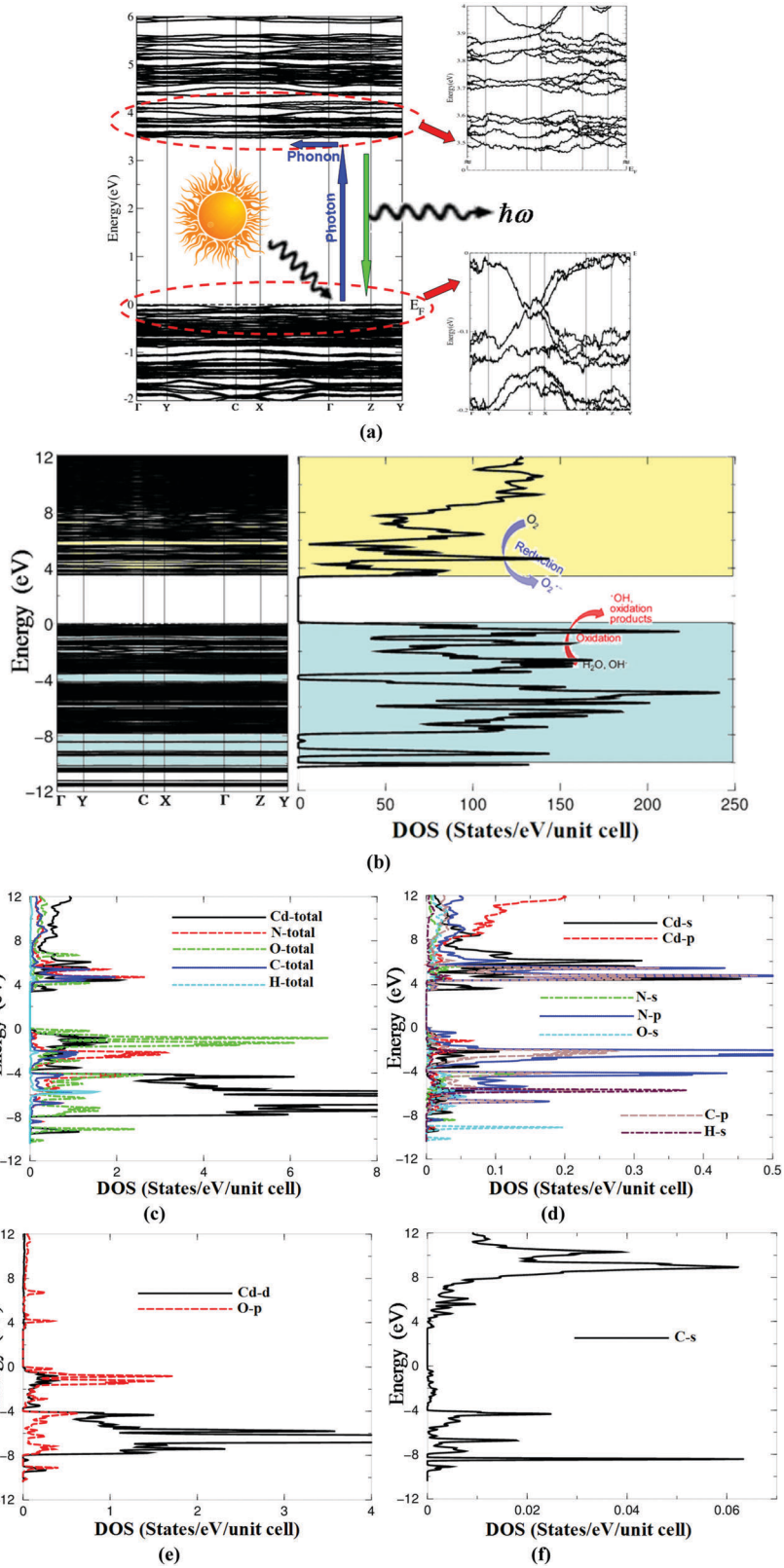

Fig. 2 (a) The calculated electronic band structure of cadmium benzoate ($(Cd(C_7H_5O_2)_2)_3(CH_3CN)_1$) which clearly shows the conduction band minimum, the valence band maximum and the energy band gap. (b) The calculated electronic band structure along with the total density of states. (c–f) Calculated partial densities of states of cadmium benzoate ($(Cd(C_7H_5O_2)_2)_3(CH_3CN)_1$) which show the orbitals that form the VBM and the CBM. They also show the hybridizations between the orbitals.

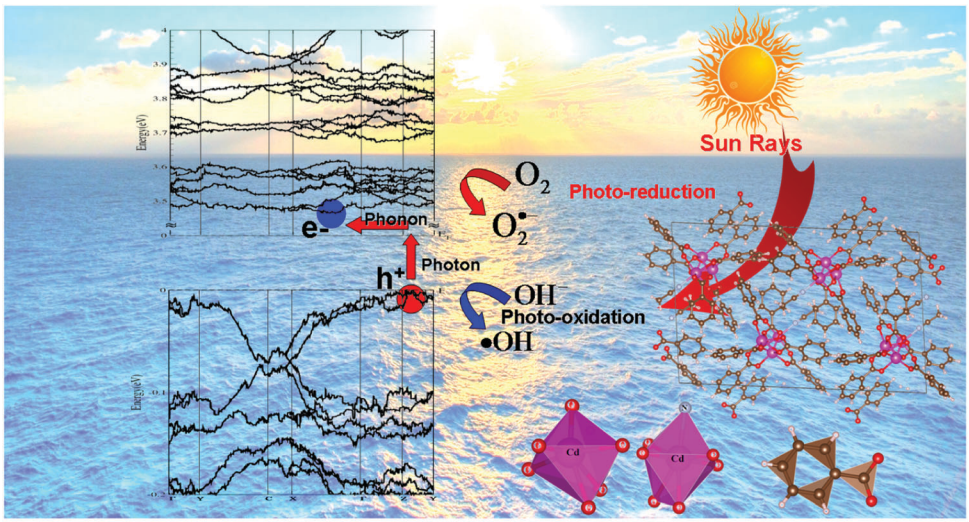

Fig. 3 (a) Schematic diagrams of charge transfer and the photocatalytic mechanism in cadmium benzoate ($(Cd(C_7H_5O_2)_2)_3(CH_3CN)_1$). When the photocatalyst absorbs radiation from sunlight, it produces electron and hole pairs. The electron of the valence band becomes excited when illuminated by light. The excess energy of this excited electron promoted the electron to the conduction band, thus creating a negative electron (e^-) and positive hole (h^+) pair. This stage is referred to as the semiconductor's 'photo-excitation' state. (b) Schematic illustration of the photocatalytic H_2 evolution mechanism for a wide energy gap semiconductor incorporated with QDs under visible light irradiation. It illustrates the mediating role of the QDs in storing and shuttling photogenerated electrons from the QDs to the wide energy gap semiconductor support in a photocatalytic process under visible light. The QDs absorb visible light and e–h pairs are formed in the CBs/VBs. The photogenerated electrons are transferred from the QDs to the wide energy gap semiconductor, where they react directly with H_2O to produce H_2. Through this mechanism, the QDs act as visible light sensitizers, to transfer photogenerated electrons from the QDs to the wide energy gap semiconductor.

light absorbed (see Fig. 3a and b); the optical absorption induces the transfer of e from the VB → CB, generating e^-–h^+ pairs which can then migrate to the surface to participate in oxidation and reduction reactions, respectively.[76,88] Usually the locations of the VBM and the CBM determine the oxidation and reduction capabilities of photogenerated holes and electrons, respectively,[76] the reduction potential level of the electron-acceptors should be energetically below the CBM, whereas the oxidization potential level of the electron-donors should be above the VBM.[89]

The optical band gap value of the semiconductor materials can be estimated from the absorption spectrum, as shown in Fig. 4a. From the absorption spectrum, the optical band gap value of the semiconductor can be solved as follows: the square of the absorption coefficient $I(\omega)$ is linear with energy (E) for direct optical transitions in the absorption edge region, whereas the square root of $I(\omega)$ is linear with E for indirect optical transitions.[63] The data plots of $[I(\omega)]^{1/2}$ *versus* E and $[I(\omega)]^2$ *versus* energy in the absorption edge region are shown in the inset of Fig. 4b and c. It is clearly shown that $[I(\omega)]^2$ *vs.* E is linear in the absorption edge region, while $[I(\omega)]^{1/2}$ *vs.* E deviates from the fitted straight line. These plots suggest that the absorption edge of the investigated material is caused by direct transitions. From Fig. 4b, we can conclude that the absorption edge of the investigated material occurs at $\lambda = 469.6$ nm, and the optical band gaps are estimated ($\lambda_g = 1239.8/E_{g(optical)}$[90]) to be 2.64 eV for cadmium benzoate ($(Cd(C_7H_5O_2)_2)_3(CH_3CN)_1$). Therefore, it can be deduced that the enhanced visible-light-driven photocatalytic activity of cadmium benzoate ($(Cd(C_7H_5O_2)_2)_3(CH_3CN)_1$) is associated with the plasmon photosensitization of QDs. The incorporation of QDs significantly extended the light absorption range to the

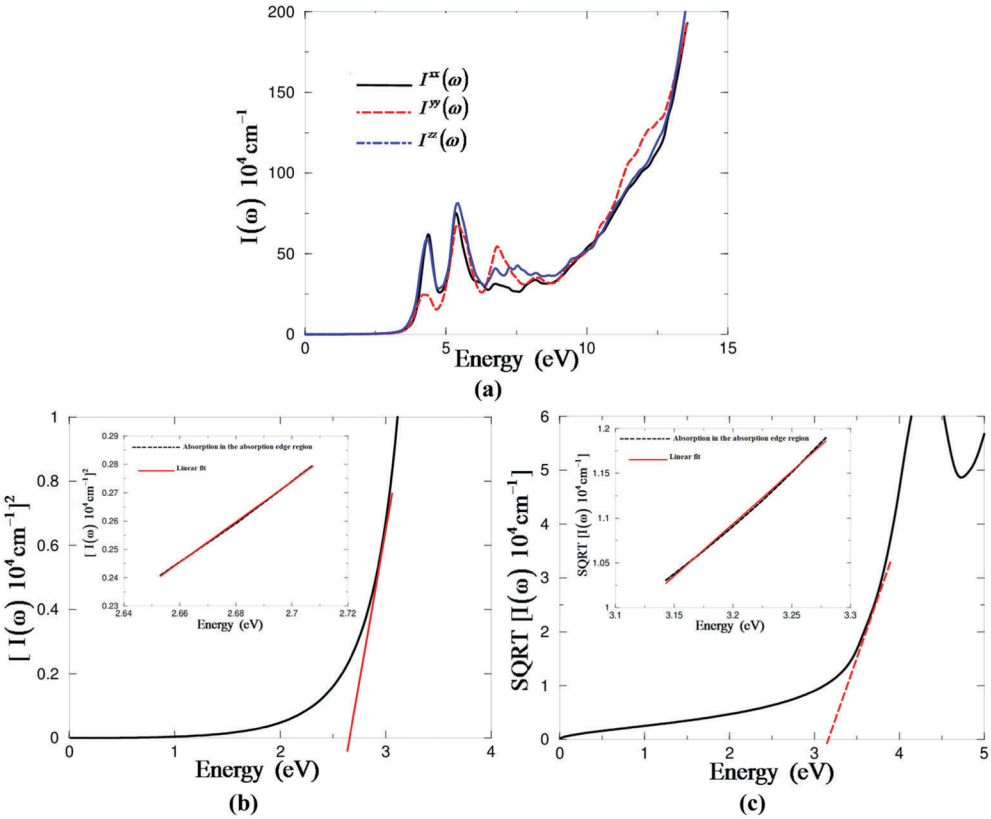

Fig. 4 (a) Calculated absorption coefficient of cadmium benzoate ($(Cd(C_7H_5O_2)_2)_3(CH_3CN)_1$) – it is clear that direct band gap semiconductors have large absorption coefficients (10^4–10^5 cm^{-1}). (b and c) The optical band gap's value of the semiconductor materials could be solved as follows; the square of the absorption coefficient $I(\omega)$ is linear with energy (E) for direct optical transitions in the absorption edge region, whereas the square root of $I(\omega)$ is linear with E for indirect optical transitions. The data plots of the square root of $I(\omega)$ *versus* E and the square root of $I(\omega)$ *versus* energy in the absorption edge region. It is clearly shown that the $[I(\omega)]^2$ *vs.* E is linear in the absorption edge region, while $[I(\omega)]^{1/2}$ *vs.* E deviates from the fitted straight line. These plots suggest that the absorption edge of the investigated materials is caused by direct transitions. The absorption edge of the investigated material occurs at λ = 469.6 nm, and the optical band gaps are estimated to be 2.64 eV for cadmium benzoate ($(Cd(C_7H_5O_2)_2)_3(CH_3CN)_1$).

visible region, which would activate their photocatalytic performance under visible light irradiation. When the QDs are directly deposited on a wide band gap semiconductor, they act as plasmonic photosensitizers to enhance the response to visible light, and can also facilitate the electron transfer from the QDs to the wide band gap semiconductor caused by the lower CBM level of the semiconductor. The combination of CdO QDs and a wide band gap semiconductor facilitates the transport of charges photogenerated under visible light irradiation; the resulting composite photocatalyst exhibits superior activity in visible-light-driven photocatalytic H_2 evolution. Therefore, we should emphasize that the amount of CdO QDs is not enough to dominate the absorption and, hence, the absorption of CdO–cadmium benzoate is still important.

3.2. Photoelectrochemical properties

It has been reported that the mobility of the electrons generated in the photocatalyst can be directly monitored by the generated photocurrent, and the generation rate should directly correlate with the photosensitivity of the material which can be used as a photocatalyst.[91] The generated large photocurrent usually signifies a high separation efficiency of e^- and h^+ pairs.[65] For an efficient photocatalytic mechanism, a material with high mobility carriers is required. To achieve this, a material with small effective masses is needed. It has been noticed from the electronic band structure (Fig. 2a) that the high k-dispersion bands around the Fermi level (E_F) possess low effective masses and, hence, the high mobility carriers (see Table 1), which enhances the charge transfer process; the effective mass provides essential information about the photocatalytic mechanism. The mobility of the photogenerated carriers significantly influences the photocatalytic efficiency[92,93] and the higher photogenerated carriers' mobility enhances the photocatalytic performance.[94–98] Moreover, the great effective mass difference (see Table 1) between electrons (e^-) and holes (h^+) can facilitate the e and h^+ migration and separation, and finally improve the photocatalytic performance.[95–98] The effective mass of h^+ is bigger than that of e^-. Therefore, the mobility of e^- is much higher than that of h^+, which consequently results in a striking difference in the mobility between the photoexcited e^-

Table 1 Calculated effective masses

m_e^*/m_o	m_h^*/m_o	$D = m_e^*/m_h^*$	$D = m_h^*/m_e^*$
0.0299	0.0036	8.3055	0.1204

and h^+. This character is beneficial in suppressing the recombination of the e^-–h^+ pairs and improving the photocatalytic efficiency.[95–98] The mobility of photoexcited carriers can be indirectly assessed by their effective masses ($\eta_e = e\tau_e/m_e^*$ and $\eta_h = e\tau_h/m_h^*$); here we call the mobility as η in order to distinguish between the mobility and chemical potential (μ). The large mobility difference is useful for the separation of e^- and h^+, the reduction of the e^- and h^+ recombination rate, and the improvement of the photocatalytic activity.[95–98] It is clear that the effective mass of the e^- is much smaller than that of h^+, and thus, one can deduce that the photogenerated carriers can fast transfer along different directions. Fig. 5a shows the carriers' mobility as a function of carrier concentration (n), which clearly shows a significant reduction in the carriers' mobility with an increase in the carrier concentration due to the increase in the scattering. To support this statement, we investigated the carriers' mobility as a function of temperature, as shown in Fig. 5b. It clearly shows a significant reduction in the carriers' mobility with an increase in the temperature, which is

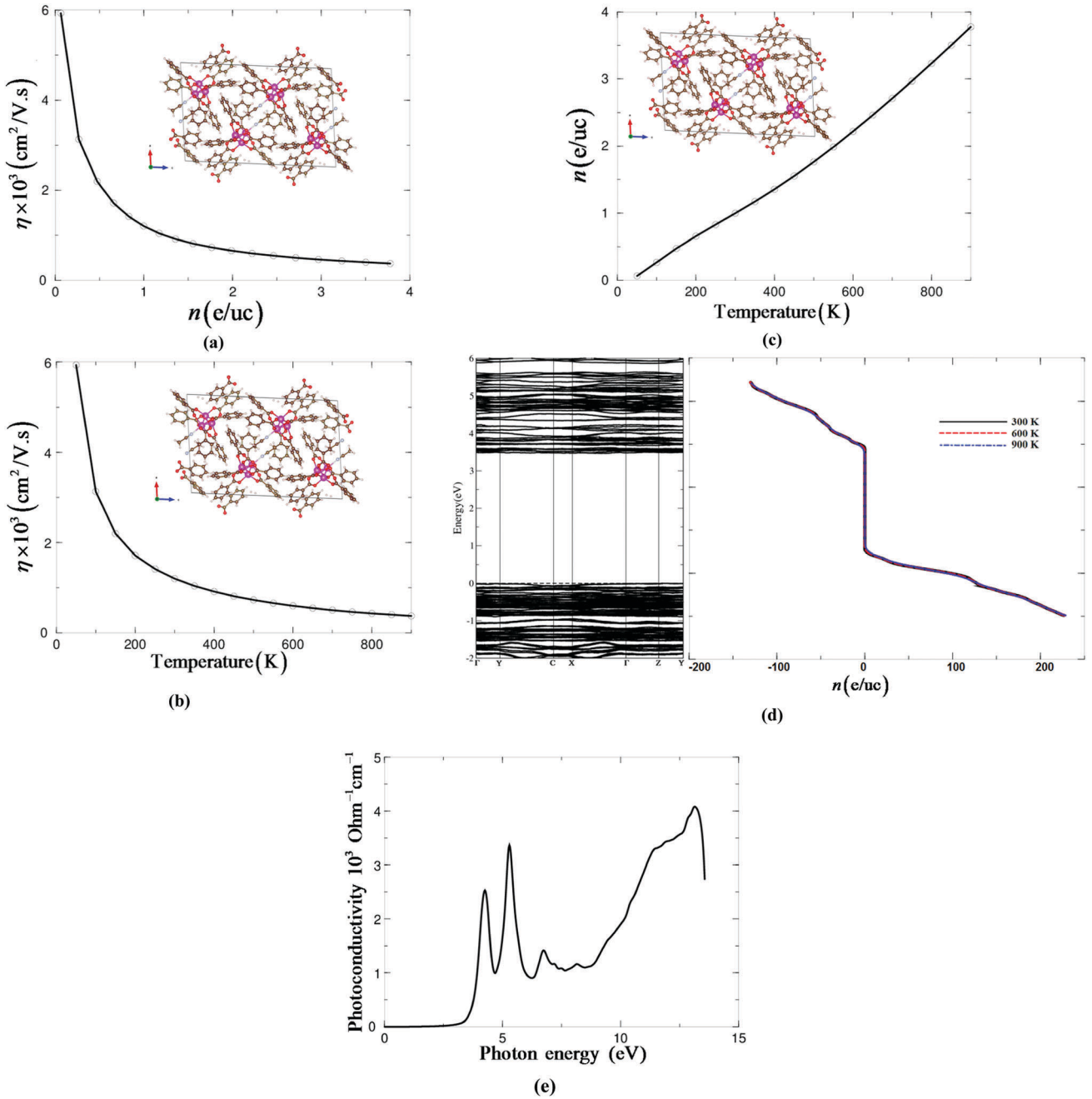

Fig. 5 (a) The mobility of cadmium benzoate ($(Cd(C_7H_5O_2)_2)_3(CH_3CN)_1$) as a function of carrier concentration; (b) the mobility of cadmium benzoate ($(Cd(C_7H_5O_2)_2)_3(CH_3CN)_1$) as a function of temperature; (c) the carrier concentration of cadmium benzoate ($(Cd(C_7H_5O_2)_2)_3(CH_3CN)_1$) as a function of temperature; (d) the carrier concentration of cadmium benzoate ($(Cd(C_7H_5O_2)_2)_3(CH_3CN)_1$) as a function of chemical potential $\mu - E_F$ at room temperature and two other randomly selected temperatures; and (e) the photoconductivity of cadmium benzoate as a function of photon energy.

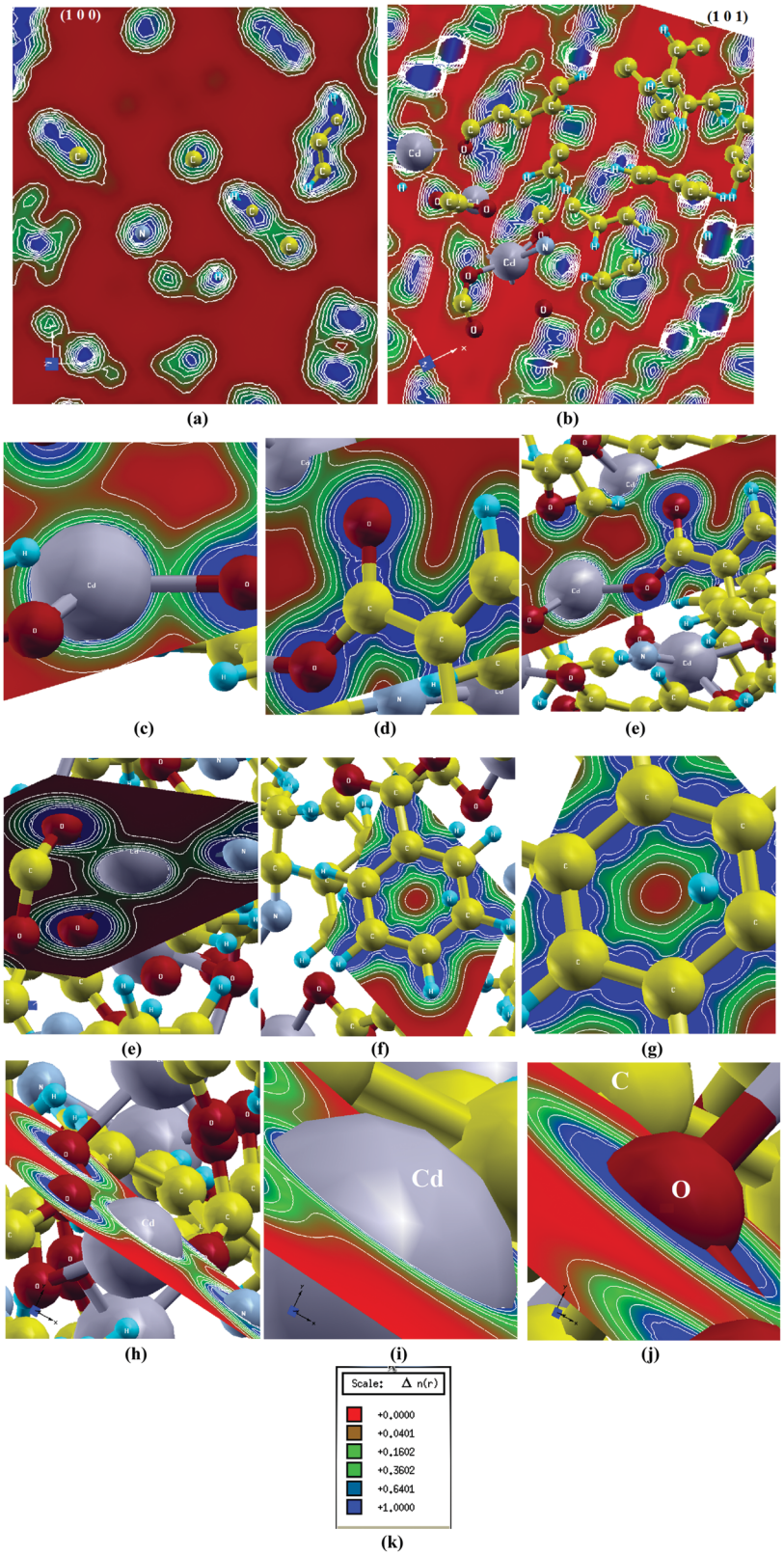

Fig. 6 (a) The charge density distribution of $(Cd(C_7H_5O_2)_2)_3(CH_3CN)_1$ in (1 0 0); (b) the charge density distribution of $(Cd(C_7H_5O_2)_2)_3(CH_3CN)_1$ in (1 0 1); (c–j) charge density distributions in different directions which show that an efficient charge transfer occurs towards O and N atoms, as the N and O atoms are surrounded by uniform spheres of charge density and the maximum charge accumulates around the O and N atoms as indicated by the blue color; and (k) thermoscale shows that the blue color indicates the maximum charge intensity (1.0000).

attributed to the fact that increasing the temperature causes the vibration to increase, and hence the mobility, resulting in an increase in the scattering which leads to the suppression of the mobility.

The other crucial issue in understanding the photocatalytic mechanism in cadmium benzoate ($(Cd(C_7H_5O_2)_2)_3(CH_3CN)_1$) is the carriers' concentration (n) and their mobility. Therefore, we investigated the influence of the temperature (T) on the carriers' concentration (n) of cadmium benzoate ($(Cd(C_7H_5O_2)_2)_3(CH_3CN)_1$) at a certain value of the chemical potential ($\mu = E_F$). It is clear that the carriers' concentration (Fig. 5c) shows a slight deviation from the linear temperature dependence. To support this statement, we investigated the n as a function of the chemical potential in the vicinity of E_F at three T values, as shown in Fig. 5d. It has been noticed that the difference between the chemical potential and the Fermi energy ($\mu - E_F$) is positive for VBs and negative for CBs, and cadmium benzoate ($(Cd(C_7H_5O_2)_2)_3(CH_3CN)_1$) exhibits a maximal n in the vicinity of E_F. Furthermore, the photoconductivity as a function of photon energy is investigated, as shown in Fig. 5e. It is clear that cadmium benzoate shows the highest photoconductivity when the photons possess an energy of about 2.64–6.5 eV and 11.0–13.5 eV. Thus, it covers the visible region. Apparently, the photocurrent was generated immediately at the absorption edge, *i.e.* 2.64 eV, which implies that cadmium benzoate exhibits a photocurrent response in the visible light region; this indicates that the investigated material may exhibit good photocatalytic activity and agrees well with the foregoing photocatalytic activity measurement.

3.3. Electronic charge density

In order to reveal the chemical bonding properties of cadmium benzoate ($(Cd(C_7H_5O_2)_2)_3(CH_3CN)_1$), the electronic charge density is calculated in two crystallographic planes, (1 0 0) and (1 0 1), as shown in Fig. 6(a–j). The charge localizes mainly between Cd and the neighboring O, also between C and O atoms, indicating partial ionic and strong covalent bonding. The strength of the interactions between the atoms is due to the degree of the hybridization and the electronegativity differences. According to the Pauling scale, the electronegativities of C, H, N, Cd and O are 2.55, 2.20, 3.04, 1.69 and 3.44, respectively. To describe the character of the chemical bonding in cadmium benzoate ($(Cd(C_7H_5O_2)_2)_3(CH_3CN)_1$), the difference of the electronegativity (X_A–X_B) is crucial,[67] where X_A and X_B denote the electronegativities of the A and B atoms in general. With an increase in the (X_A–X_B) difference, the ionic character (P) of the bonding increases. The percentage of P for the chemical bonding can be obtained using the expression:[99]

$$P\,(\%) = 16(X_A - X_B) + 3.5(X_A - X_B)^2 \quad (3)$$

The calculated values of P are given in Table 2. It is clear that the Cd–O, C–O, Cd–N and C–N bonds are mostly covalent and partially ionic, see Table 2. The covalent bonding is more favorable for the transport of the carriers than ionic bonding.[100] Also, due to the electronegativity differences between the atoms, some valence electrons are transferred to the O atoms, as it is clear that these atoms are surrounded by uniform blue spheres, which indicate the maximum charge accumulation according to the thermoscale (Fig. 6k). The Cd–O, C–O, Cd–N and C–N bonds possess strong electron cloud overlap and prefer to attract holes and repel electrons, thus facilitating the separation of the photogenerated e–h^+ pairs. This in turn enhances the photocatalytic activity.[101]

Table 2 The calculated values of the ionic character of cadmium benzoate ($(Cd(C_7H_5O_2)_2)_3(CH_3CN)_1$)

Bonds	P (%)
Cd–O	38.71
C–O	17.01
C–N	8.68
Cd–N	27.97

4. Conclusion

The remarkably enhanced photocatalytic performance of cadmium benzoate can be attributed to the incorporation of CdO QDs. The introduction of CdO QDs improves the absorption level to the visible region and significantly strengthens the separation between photogenerated carriers. The estimated optical band gap of cadmium benzoate is 2.64 eV, and the EPc and EPv are about −0.09 V (*vs.* NHE) and +2.55 V (*vs.* NHE), respectively. Thus, cadmium benzoate possesses a high negative reduction potential of excited electrons due to its higher CB position, and hence, the locations of the CBM and VBM accommodate the redox capacity. Thus, the composite photocatalyst exhibits superior activity in visible-light-driven photocatalytic H_2 evolution under visible light irradiation. The electronic band structure of cadmium benzoate shows high k-dispersion bands around E_F, which implies low effective masses and, hence, the high mobility carriers enhance the charge transfer process. It was found that cadmium benzoate possesses a great effective mass difference between e^- and h^+, which can facilitate the e^- and h^+ migration and separation, and finally improve the photocatalytic performance. The large mobility difference is useful for the separation of e^- and h^+, reduction of the e^- and h^+ recombination rate, and improvement of the photocatalytic activity. Thus, cadmium benzoate is proved to be a good photocatalyst due to the rapid generation of e^-–h^+ pairs with photoexcitation, and a high negative reduction potential of excited electrons due to its higher CB position. Based on these results one can conclude that cadmium benzoate satisfied all requirements to be an efficient photocatalyst.

Author contribution

A. H. Reshak, a professor with PhD in physics and PhD in materials engineering, performed the calculations and contributed to analyzing and discussing the results and writing the manuscript.

Conflicts of interest

The author declares no competing financial interests.

Acknowledgements

This work was developed within the CENTEM project, reg. no. CZ.1.05/2.1.00/03.0088, co-funded by the ERDF as part of the Ministry of Education, Youth and Sports OP RDI program and, in the follow-up sustainability stage, supported through CENTEM PLUS (LO1402) by financial means from the Ministry of Education, Youth and Sports under the "National Sustainability Programme I. Computational resources were provided by MetaCentrum (LM2010005) and CERIT-SC (CZ.1.05/3.2.00/08.0144) infrastructures.

References

1 J. Schneider, M. Matsuoka, M. Takeuchi, J. Zhang, Y. Horiuchi, M. Anpo and D. W. Bahnemann, *Chem. Rev.*, 2014, **114**, 9919–9986.
2 A. L. Linsebigler, G. Lu and J. T. Yates Jr, *Chem. Rev.*, 1995, **95**, 735–758.
3 X. Chen and S. S. Mao, *Chem. Rev.*, 2007, **107**, 2891–2959.
4 T. Tachikawa, M. Fujitsuka and T. Majima, *J. Phys. Chem. C*, 2007, **111**, 5259–5275.
5 S. Yu, Y. H. Kim, S. Y. Lee, H. D. Song and J. Yi, *Angew. Chem., Int. Ed.*, 2014, **126**, 11385–11389.
6 H. Tada, T. Mitsui, T. Kiyonaga, T. Akita and K. Tanaka, *Nat. Mater.*, 2006, **5**, 782–786.
7 H. Zhu, B. Yang, J. Xu, Z. Fu, M. Wen, T. Guo, S. Fu, J. Zuo and S. Zhang, *Appl. Catal., B*, 2009, **90**, 463–469.
8 J. Fang, L. Xu, Z. Zhang, Y. Yuan, S. Cao, Z. Wang, L. Yin, Y. Liao and C. Xue, *ACS Appl. Mater. Interfaces*, 2013, **5**, 8088–8092.
9 H. Zhou, L. Ding, T. Fan, J. Ding, D. Zhang and Q. Guo, *Appl. Catal., B*, 2014, **147**, 221–228.
10 M. Kim, Y. K. Kim, S. K. Lim, S. Kim and S.-I. In, *Appl. Catal., B*, 2015, **166**, 423–431.
11 H. Zhao, M. Wu, J. Liu, Z. Deng, Y. Li and B.-L. Su, *Appl. Catal., B*, 2016, **184**, 182–190.
12 S. Linic, P. Christopher and D. B. Ingram, *Nat. Mater.*, 2011, **10**, 911–921.
13 Y. Tian and T. Tatsuma, *J. Am. Chem. Soc.*, 2005, **127**, 7632–7637.
14 H. Li, Z. Bian, J. Zhu, Y. Huo, H. Li and Y. Lu, *J. Am. Chem. Soc.*, 2007, **129**, 4538–4539.
15 J. Li, S. K. Cushing, P. Zheng, T. Senty, F. Meng, A. D. Bristow, A. Manivannan and N. Wu, *J. Am. Chem. Soc.*, 2014, **136**, 8438–8449.
16 M. Stock and S. Dunn, *J. Phys. Chem. C*, 2012, **116**, 20854.
17 (*a*) Y. Inoue, K. Sate, K. Sato and H. Miyama, *J. Phys. Chem.*, 1986, **90**, 2809; (*b*) L. Li, P. A. Salvador and G. S. Rohrer, *Nanoscale*, 2014, **6**, 24; (*c*) M. E. Lines and A. M. Glass, *Principles and Applications of Ferroelectrics and Related Materials*, Clarendon Press, Oxford, UK, 2001.
18 M. T. Buelow and A. J. Gellman, *J. Am. Chem. Soc.*, 2001, **123**, 1440.
19 C. Gomes Silva, R. Juarez, T. Marino, R. Molinari and H. Garcia, *J. Am. Chem. Soc.*, 2011, **133**, 595–602.
20 W. C. W. Chan, D. J. Maxwell, X. H. Gao, R. E. Bailey, M. Y. Han and S. M. Nie, *Curr. Opin. Biotechnol.*, 2002, **13**, 40.
21 H. R. Rajabi, Photocatalytic Activity of Quantum Dots, chapter 17 Semiconductor Photocatalysis – Materials, Mechanisms and Applications: http://www.intechopen.com/books/semiconductor-photocatalysismaterials-mechanisms-and-applications.
22 A. Kubacka, M. Fernández-García and G. Colón, *Chem. Rev.*, 2012, **112**, 1555.
23 X. J. Bai, L. Wang, Y. J. Wang, W. Q. Yao and Y. F. Zhu, *Appl. Catal., B*, 2014, **262**, 152–153.
24 A. Hagfeldt and M. Gratzel, *Chem. Rev.*, 1995, **95**, 49.
25 Y. Wang, Z. Zhang and Y. Zhu, *et al.*, *ACS Nano*, 2008, **2**, 1492–1496.
26 G. N. Schrauzer and T. D. Guth, *J. Am. Chem. Soc.*, 1977, **99**, 7189–7193.
27 X. Chen, T. Yu and X. Fan, *et al.*, *Appl. Surf. Sci.*, 2007, **253**, 8500–8506.
28 K. Maeda, N. Saito, D. Lu, Y. Inoue and K. Domen, *J. Phys. Chem. C*, 2007, **111**, 4749–4755.
29 J. S. Jang, S. H. Choi, D. H. Kim, J. W. Jang, K. S. Lee and J. S. Lee, *J. Phys. Chem. C*, 2009, **113**, 8990–8996.
30 K. Domen, A. Kudo, M. Shibata, A. Tanaka, K. I. Maruya and T. Onishi, *J. Chem. Soc., Chem. Commun.*, 1986, **23**, 1706–1707.
31 B. L. Cushing, V. L. Kolesnichenko and C. J. ÓConnor, *Chem. Rev.*, 2004, **104**, 3893.
32 R. B. Waghulade, P. P. Patil and R. Pasricha, *Talanta*, 2007, **72**, 594.
33 G. N. Chaudhari, A. M. Bende, A. B. Bodade, S. S. Patil and V. S. Sapkal, *Sens. Actuators, B*, 2006, **115**, 297.
34 A. Srivastava, K. Jain, Rashmi, A. K. Srivastava and S. T. Lakshmikumar, *Mater. Chem. Phys.*, 2006, **97**, 85.
35 G. N. Chaudhari, A. M. Bende, A. B. Bodade, S. S. Patil and S. V. Manorama, *Talanta*, 2006, **69**, 187.
36 C. Aifan, H. Xiaodong, T. Zhangfa, B. Shouli, L. Ruixian and L. C. Chiun, *Sens. Actuators, B*, 2006, **115**, 316.
37 C. H. Champness, K. Ghoneim and J. K. Chen, *Can. J. Phys.*, 1985, **63**, 767.
38 L. M. Su, N. Grote and F. Schmitt, *Electron. Lett.*, 1984, **20**, 716.
39 L. M. Su, N. Grote and F. Schmitt, *Electron. Lett.*, 1984, **20**, 717.
40 I. M. Ocampo, A. M. Ferandez and P. J. Sabastian, *Semicond. Sci. Technol.*, 1993, **8**, 750.
41 F. A. Benko and F. P. Koffyberg, *Solid State Commun.*, 1986, **57**, 901.
42 K. Gurumugan, D. Mangalarag, S. K. Narayandass, K. Sekar and C. P. Girija Vallabham, *Semicond. Sci. Technol.*, 1994, **9**, 1827.
43 C. Xiangfeng, L. Xingqin and M. Guangyao, *Sens. Actuators, B*, 2000, **65**, 64.
44 R. S. Mane, H. M. Pathan, C. D. Lokhande and S.-H. Han, *Sol. Energy*, 2006, **80**, 185.
45 T. Goldacker, V. Abetz, R. Stadler, I. Erukhimovich and L. Leibler, *Nature*, 1999, **398**, 137.

46 Y. Cui, J. Briscoe and S. Dunn, *Chem. Mater.*, 2013, **25**, 4215.
47 S. V. Kalinin and D. A. Bonnell, *Nanoscale Phenomena in Ferroelectric Thin Films*, Kluwer Academic Publications, Dordrecht, The Netherlands, 2004, pp. 182–216.
48 S. Dunn, P. M. Jones and D. E. Gallardo, *J. Am. Chem. Soc.*, 2007, **129**, 8724.
49 M. W. Kanan and D. G. Nocera, *Science*, 2008, **321**, 1072–1075.
50 H. Tong, S. X. Ouyang, Y. P. Bi, N. Umezawa, M. Oshikiri and J. H. Ye, *Adv. Mater.*, 2012, **24**, 229–251.
51 A. Kubacka, M. Fernández-García and G. Colón, *Chem. Rev.*, 2012, **112**, 1555–1614.
52 M. Muruganandham, R. Amutha, G. J. Lee, S. H. Hsieh, J. J. Wu and M. Sillanpää, *J. Phys. Chem. C*, 2012, **116**, 12906–12915.
53 L. Huang, X. L. Wang, J. H. Yang, G. Liu, J. F. Han and C. Li, *J. Phys. Chem. C*, 2013, **117**, 11584–11591.
54 S. J. Li, S. M. Liu, S. X. Liu, Y. W. Liu, Q. Tang, Z. Shi, S. X. Ouyang and J. H. Ye, *J. Am. Chem. Soc.*, 2012, **134**, 19716–19721.
55 T. Wen, D. X. Zhang and J. Zhang, *Inorg. Chem.*, 2013, **52**, 12–14.
56 A. N. Beecher, X. Yang, J. H. Palmer, A. L. LaGrassa, P. Juhas, S. J. L. Billinge and J. S. Owen, *J. Am. Chem. Soc.*, 2014, **136**, 10645–10653.
57 Z. Zhang, T. Zheng, X. Li, J. Xu and H. Zeng, *Part. Part. Syst. Charact.*, 2016, **33**, 457–472.
58 Q. Gu, H. Zhuang, J. Long, X. An, H. Lin, H. Lin and X. Wang, *Int. J. Photoenergy*, 2012, **2012**, 857345.
59 P. Blaha, K. Schwarz, G. K. H. Madsen, D. Kvasnicka and J. Luitz, *WIEN2k, An augmented plane wave plus local orbitals program for calculating crystal properties*, Vienna University of Technology, Austria, 2001.
60 J. P. Perdew, S. Burke and M. Ernzerhof, *Phys. Rev. Lett.*, 1996, **77**, 3865.
61 F. Tran and P. Blaha, *Phys. Rev. Lett.*, 2009, **102**, 226401.
62 V. V. Atuchin, T. A. Gavrilova, J.-C. Grivel and V. G. Kesler, *Surf. Sci.*, 2008, **602**, 3095–3099; V. V. Atuchin, T. A. Gavrilova, J.-C. Grivel and V. G. Kesler, *J. Phys. D: Appl. Phys.*, 2009, **42**, 035305; O. Y. Khyzhun, V. L. Bekenev, V. V. Atuchin, E. N. Galashov and V. N. Shlegel, *Mater. Chem. Phys.*, 2013, **140**, 558–595; V. V. Atuchin, E. N. Galashov, O. Y. Khyzhun, V. L. Bekenev, L. D. Pokrovsky, Y. A. Borovlev and V. N. Zhdankov, *J. Solid State Chem.*, 2016, **236**, 24–31.
63 H. Huang, X. Han, X. Li, S. Wang, P. K. Chu and Y. Zhang, *ACS Appl. Mater. Interfaces*, 2015, **7**, 482–492; H. Huang, X. Li, J. Wang, F. Dong, P. K. Chu, T. Zhang and Y. Zhang, *ACS Catal.*, 2015, **5**, 4094–4103.
64 H. Huang, Y. He, X. Li, M. Li, C. Zeng, F. Dong, X. Du, T. Zhangd and Y. Zhang, *J. Mater. Chem. A*, 2015, **3**, 24547–24556; H. Huang, Y. He, Z. Lin, L. Kang and Y. Zhang, *J. Phys. Chem. C*, 2013, **117**, 22986–22994.
65 (*a*) H. Zhang, L. Liua and Z. Zhou, *Phys. Chem. Chem. Phys.*, 2012, **14**, 1286–1292; (*b*) J. Zhang, P. Zhou, J. Liu and J. Yu, *Phys. Chem. Chem. Phys.*, 2014, **16**, 20382.
66 J. Zhang, W. Yu, J. Liu and B. Liud, *Appl. Surf. Sci.*, 2015, **358**, 457–462.
67 X. Li, J. Zhao and J. Yang, *Sci. Rep.*, 2013, **3**, 1858.
68 D. W. Hwang, J. S. Lee, W. Li and S. H. Oh, *J. Phys. Chem. B*, 2003, **107**, 4963–4970.
69 C. Liu, Y. Zhang, F. Dong, A. H. Reshak, L. Ye, N. Pinna, C. Zeng, T. Zhang and H. Huang, *Appl. Catal., B*, 2017, **203**, 465–474; H. Huang, S. Tu, C. Zeng, T. Zhang, A. H. Reshak and Y. Zhang, *Angew. Chem., Int. Ed.*, 2017, **56**, 1–6.
70 A. H. Reshak, *J. Catal.*, 2017, **352**, 142–154.
71 A. H. Reshak, *J. Catal.*, 2017, **351**, 119–129.
72 A. H. Reshak and S. Auluck, *J. Catal.*, 2017, **351**, 1–9.
73 P. Zhou, J. H. Wu, W. L. Yu, G. H. Zhao, G. J. Fang and S. W. Cao, *Appl. Surf. Sci.*, 2014, **319**, 167–172.
74 M. C. Xu, Y. K. Gao, E. M. Moreno, M. Kunst, M. Muhler, Y. Wang, H. Idriss and C. Wo, *Phys. Rev. Lett.*, 2011, **106**, 138302.
75 J. F. Zhang, P. Zhou, J. J. Liu and J. G. Yu, *Phys. Chem. Chem. Phys.*, 2014, **16**, 20382–20386.
76 J. Zhang, W. Yu, J. Liu and B. Liu, *Appl. Surf. Sci.*, 2015, **358**, 457–462.
77 M. Roushani, M. Mavaei and H. R. Rajabi, *J. Mol. Catal. A: Chem.*, 2015, **409**, 102.
78 S. S. Khan, *J. Photochem. Photobiol., B*, 2015, **142**, 1–7.
79 L. Sun, D. Zhao, Z. Song, C. Shan, Z. Zhang, B. Li and D. Shen, *J. Colloid Interface Sci.*, 2011, **363**, 175–181.
80 J.-Z. Kong, A.-D. Li, H.-F. Zhai, Y.-P. Gong, H. Li and D. Wu, *J. Solid State Chem.*, 2009, **182**, 2061–2067.
81 Y. Zong, Z. Li, X. Wang, J. Ma and Y. Men, *Ceram. Int.*, 2014, **40**, 10375–10382.
82 M. Jakob, H. Levanon and P. V. Kamat, *Nano Lett.*, 2003, **3**, 353–358.
83 J. S. Curran and D. Lamouche, *J. Phys. Chem.*, 1983, **87**, 5405–5411.
84 A. Wood, M. Giersig and P. Mulvaney, *J. Phys. Chem. B*, 2001, **105**, 8810–8815.
85 Y. Matsumoto, *J. Solid State Chem.*, 1996, **126**, 227–234.
86 D. Dvoranová, V. Brezová and M. Mazúra, *et al.*, *Appl. Catal., B*, 2002, **37**, 91–105.
87 D. Beydoun, R. Amal, G. Low and S. McEvoy, *J. Nanopart. Res.*, 1999, **1**, 439.
88 J. C. Wu, J. W. Zheng, P. Wu and R. Xu, *J. Phys. Chem. C*, 2011, **115**, 5675–5682.
89 S. Banerjee, J. Gopal, P. Muraleedharan, A. K. Tyagi and B. Raj, *Curr. Sci.*, 2006, **90**, 1378–1383.
90 J. M. Carlsson, B. Hellsing, H. S. Domingos and P. D. Bristowe, *Phys. Rev. B: Condens. Matter Mater. Phys.*, 2002, **65**, 205122.
91 H. G. Kim, P. H. Borse, W. Y. Choi and J. S. Lee, *Angew. Chem., Int. Ed.*, 2005, **44**, 4585–4589.
92 J. W. Tang and J. H. Ye, *Chem. Phys. Lett.*, 2005, **410**, 104–107.
93 T. L. Bahers, M. R. rat and P. Sautet, *J. Phys. Chem. C*, 2014, **118**, 5997–6008.
94 J. Sato, H. Kobayashi and Y. Inoue, *J. Phys. Chem. B*, 2003, **107**, 7970–7975.
95 H. J. Zhang, L. Liu and Z. Zhou, *Phys. Chem. Chem. Phys.*, 2012, **14**, 1286–1292.

96 J. F. Zhang, P. Zhou, J. J. Liu and J. G. Yu, *Phys. Chem. Chem. Phys.*, 2014, **16**, 20382–20386.
97 J. Zhang, W. Yu. J. Liu and B. Liu, *Appl. Surf. Sci.*, 2015, **358**, 457–462.
98 J. Yang, P. Jiang, M. Yue, D. Yang, R. Cong, W. Gao and T. Yang, *J. Catal.*, 2017, **345**, 236–244.
99 Schlusseltechnologien Key Technologies, 41st IFF Spring School, 2010, vol. 11, pp. A1–A18, ISBN 978-3-89336-559-3.
100 F. Wu, H. Z. Song, J. F. Jia and X. Hu, *Prog. Nat. Sci.: Mater. Int.*, 2013, **23**, 408–412.
101 X. Fan, L. Zang, M. Zhang, H. Qiu, Z. Wang, J. Yin, H. Jia, S. Pan and C. Wang, *Chem. Mater.*, 2014, **26**, 3169–3174.